Size resolved particle work function measurement of free nanoparticles: Aggregates vs. spheres

Lei Zhou, Michael R. Zachariah *

Department of Mechanical Engineering and Department of Chemistry and Biochemistry, University of Maryland, College Park 20742, USA

ARTICLE INFO

ABSTRACT

In this Letter, we employed an ion mobility technique to measure the size-resolved native work function of structure controlled nanoparticles in free flight. We found that the Fowler–Nordheim law is applicable to not only spheres but also aggregates. The measured work functions of spheres are size dependent, and consistent with classical image and Coulomb potentials explanations. On the other hand, the measured work functions of aggregates are independent of mobility size, but depend on the size of primary particles. In addition, the particle photoelectric yield of aggregates and spheres were also evaluated as function of incident photon energy.

© 2011 Published by Elsevier B.V.

1. Introduction

Photoelectric emission and work function of solid surfaces have been explored for several decades [1–3]. In recent years, nanostructured materials, such as nanoparticles, have become the center of attention because of their unexpected and often better or enhanced properties as compared to their bulk counterparts. Work function and photoelectric activity of small particles are important properties because they offer one of the direct windows to view the transition of properties from atoms to bulk materials. They also offer the opportunity to relate surface activity, as for example in catalysis, to electronic structure [4,5]. Typically, work function measurements of nanoparticles are conducted on a substrate. However, interactions between substrate and particles may alter the properties of the nanoparticles and may not represent their intrinsic surface characteristics [4,6]. There have been many advanced techniques developed to measure the native work function of unsupported nanoparticles. For example, highly sophisticated and specialized cluster beam systems have been developed to probe the photoelectric behavior and ionization potential of metal clusters [7,8]. Another family of experiments probe the photoelectric charging and particle work function through the so-called aerosol-based approaches [3,6,9–14]. In these reported aerosol based approaches, particles in gas phase are irradiated by ultraviolet (UV) light and the resulting charged particles are examined by either electrometers or through electrical mobility analysis. The aerosol based techniques have the advantage that particles are produced and manipulated in a gas stream. Therefore, their native properties can be investigated at atmospheric pressure in an on-the-fly, size-resolved manner without the interference from a substrate.

Despite off the many efforts directed to measure the photoelectric activity and work function of nanoparticles, there are still many remaining issues on how to measure and understand the native particle work function, such as on successful experiment design, appropriate data processing and analysis, and in particular, the effects of size and structure on the intrinsic work function of nanoparticles. In order to address some of these issues, we employed Differential Mobility Analysis [15–17] to evaluate photoelectric charging of structure controlled silver nanoparticles (aggregates vs. spheres) by UV photoelectric ionization in free flight.

2. Experimental

The schematic of the experimental system is shown in Figure 1. A two furnaces setup was used to generate aggregate or spherical silver nanoparticles. Silver aggregates were generated by heating bulk silver powder crystal (Alfa Aesar 99.9%) in a ceramic boat inside a tube furnace at 1050 °C under a flow of ultra high purity nitrogen. To produce spherical silver particles, the aggregates were sintered in a second furnace at 600 °C. The morphology of produced aggregate particles was further examined through Transmission Electron Microscopy (TEM), shown in Figure 2a. The TEM image of silver aggregates shows significant necking between primary particles due to coalescence at high temperature, which make the structure interpretation complicated. Here we adopted a simplified 'ideal aggregate' approach in which aggregates are composed of primary particles of the same diameter and the necking between primary particles is ignored, i.e. point contact

* Corresponding author. Fax: +1 301 314 9477.
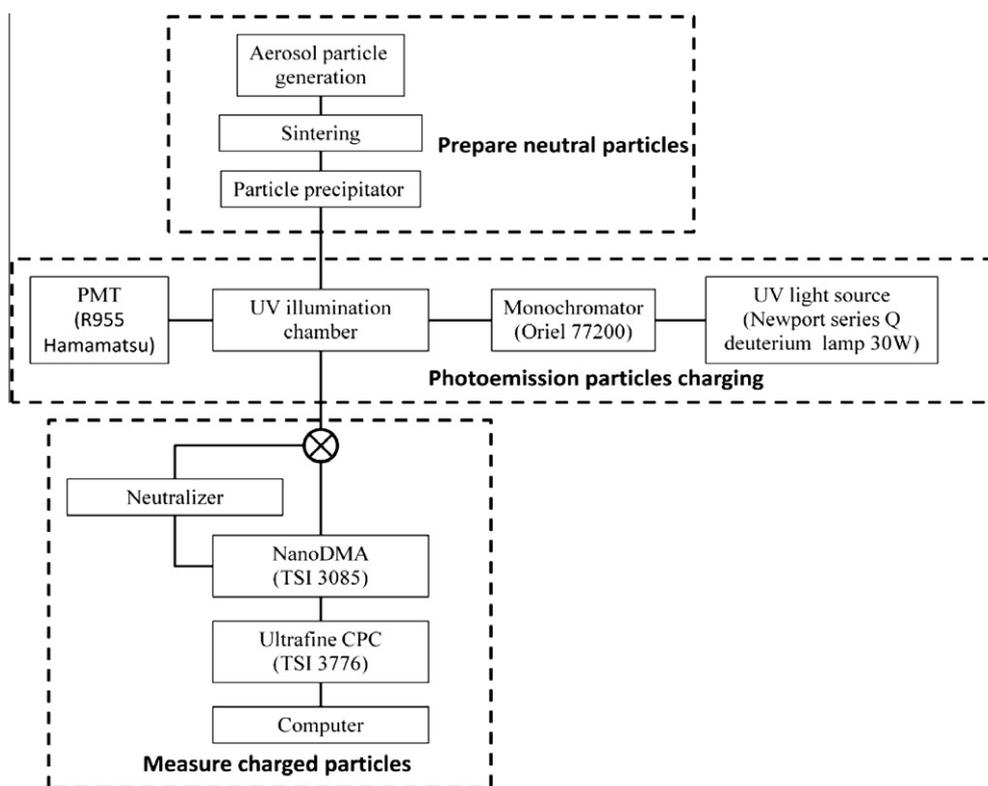E-mail addresses: mrz@umd.edu, mrz@me.umd.edu (M.R. Zachariah).

Figure 1. Schematic of experimental system for photoionization threshold measurement.
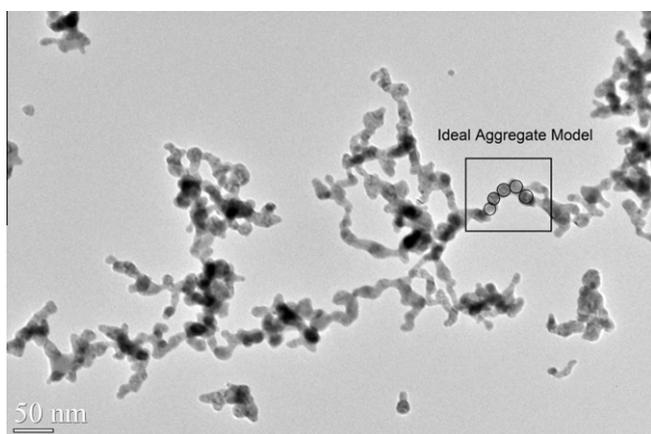

Figure 2a. TEM images of aggregate silver particles.

Figure 2b. TEM images of size resolved sphere particles, particle size is 28.5 nm based on DMA selection and 28.6 nm based on TEM measurement. TEM measurement is based on total of 139 particles.

between primary particles, as illustrated in the box area of Figure 2a. Based on the TEM image and the 'ideal aggregate' approach, we determined that the primary particle diameter in aggregates is about 15 nm. To demonstrate the size resolving power of Differential Mobility Analyzer (DMA), size resolved sintered (spherical) silver particles were also examined through TEM as shown in Figure 2b. In this TEM measurement, particles of 28.5 nm were selected by DMA and TEM measured average particle size is 28.6 nm (based on total of 139 particles). Silver particles were then passed through an electrostatic precipitator to remove any pre-existing remnant charged particles. The remaining neutral particles were sent to the photoelectric ionization chamber and exposed to UV irradiation. The photoelectric ionization chamber is a 65 cm long grounded metal tube with i.d. 3.5 cm. For a nominal flow rate of 1 l/min, the particle residence time is estimated to be ~29 s. The
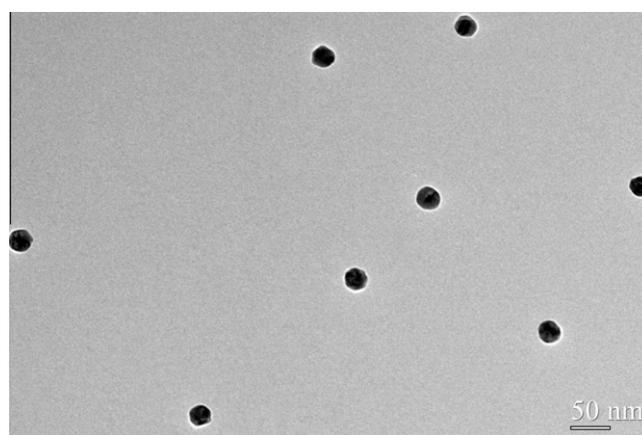
tube was fully illuminated with a collimated 3.4 cm dia UV beam produced from the light source, which consists of a 30 W deuterium lamp (Newport series Q) coupled with a monochromator (Oriel 77200) and the beam intensity was measured with a Photomultiplier tube (PMT) (Hamamatsu R955). In the experiment, UV light wavelength range from 200 to 280 nm (photon energy 6.20–4.43 eV) were selected by the monochromator for particle photoionization and the mobility spectrum of the resulting charged particles were measured through particle mobility analysis. With the light source turned off, the particles were passing through a neutralizer that gives particles a known charge distribution thus the true mobility size distribution of neutral particles can also be obtained. Comparing the photoelectric ionized particle

distribution to the neutral particle size distribution, the size resolved particle charging efficiency (CE) can be obtained. The particle mobility analysis setup consists of a Nano Differential Mobility Analyzer (NanoDMA) (TSI Incorporated model 3085) and an Ultrafine Condensation Particle Counter (CPC) (TSI Incorporated model 3776). Detailed information regarding to the operation principles of the measurement setup and its applications can be found elsewhere [16,18–20]. For our photoelectric charging experiments, we operated the UV source and monchometer such that the wavelength bandpass was between 0.7 and 3 nm (energy bandpass between 0.09 and 0.02 eV) depending on wavelength to ensure primarily single charging conditions. Nitrogen was used as the carrier gas. Hence, the formation of negative ions can be neglected such that diffusion charging should be low. This was confirmed by reversing the polarity for the mobility measurement to show that no particles were detected in the negative spectrum.

3. Results and discussion

3.1. Particle photoelectric yield

For photoemission from a macroscopic surface, the photoelectric quantum yield $Y(h\nu)$ is defined as the number of emitted photoelectrons per incident photon per unit active surface area. However, for small particles, the particle photoelectric yield $y_{particle}$, which is the number of emitted photoelectrons per incident photon per particle, is often considered and related to the quantum yield as:

$$y_{particle} \propto \sigma_{abs} Y(h\nu) \qquad (1)$$

where σ_{abs} is the particle absorption cross section, $h\nu$ is the photon energy. The behavior of quantum yield $Y(h\nu)$ is believed to follow the well known three-step model of Berglund and Spicer [21,22], which has been extended to the case of spherical particles [12,13,23]. In the vicinity of photoelectric ionization threshold ($h\nu - \Phi \leqslant \sim 1.5$ eV, which is also called the Fowler–Nordheim regime) [2], the relationship of $Y(h\nu)$ of macroscopic surface with work function Φ has the form as:

$$Y(h\nu) = c(h\nu - \Phi)^m \qquad (2)$$

The above equation is the well known Fowler–Nordheim law [2] where c is the photoelectric constant and m is 2 for metals. It has been experimentally confirmed that the Fowler–Nordheim law is also applicable to systems of finite size, such as small particles or clusters [3,24,25]. We note here that depending on the scientific community, particle work function and ionization potential are interchangeable concepts (Small cluster community [8,24,26] and aerosol/nanoparticle field [3,12,13,25]). In this Letter we will refer to work function of particles, rather than ionization potential.

In an aerosol based experiment employing an ion-mobility based method such as a DMA, from the mobility spectra of a particle population, one can extract the particle charging efficiency (CE), normalized by the illumination flux I, gives:

$$\frac{CE}{I} \propto y_{particle} \propto \sigma_{abs} Y(h\nu) \qquad (3)$$

Thus, it is possible to use Eq. (3) to experimentally evaluate the behavior of either particle photoelectric yield $y_{particle}$ or the quantum yield $Y(h\nu)$. During the course of our experiments, we found accurate evaluation requires taking into account of the multiple charging effects. To demonstrate this key point, we show measured CE/I against photon energies for various mobility particle diameters in Figure 3a and b for spheres and aggregates, respectively. Here, the experimental parameters were carefully tuned to ensure a single photoelectric charging condition. (The single charging condition
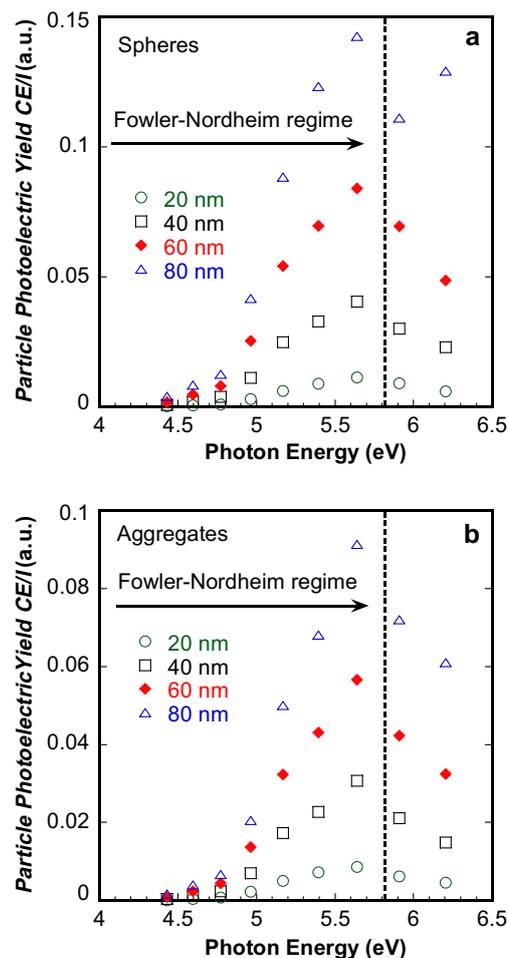

Figure 3. Measured particle photoelectric yield (normalized charging efficiency CE/I) for (a) spheres and (b) aggregates, for various mobility sizes.

is confirmed through a standard Tandem DMA measurement, description on Tandem DMA measurement can be found elsewhere) [9,16]. The observed particle photoelectric yield $y_{particle}$ of aggregates and spheres has a similar behavior. Near photoionization threshold, where the Fowler–Nordheim regime is expected to be valid ($h\nu - \Phi \leqslant \sim 1.5$ eV), the particle photoelectric yield $y_{particle}$ rises as the incident photon energy increases. However, as photon energy further increases to outside the Fowler Nordheim regime, the particle photoelectric yield starts to decrease with increasing photon energy. In a similar experiment where we allowed for multiple charging of particles, i.e. under high photon flux (multiple charging states were confirmed through a standard Tandem DMA measurement), we found a monotonic increase in the 'apparent charging efficiency' with increasing photon energy, for both spheres and aggregates. Thus the charging efficiency profile can be mistakenly considered as a monotonic function of incident photon energy if the multiple charging is not correctly accounted for. We note this point because of some discrepancies reported in the literature [7,12,27]. While the photoelectric charging profiles shown in Figure 3a and b are consistent with reported work which investigated the photoelectric behavior of alkali metals clusters [7,27], they contrast with a previous report where the particle yield of silver nanoparticles increases in the entire incident photon energy range from 4.5 to 12 eV [12]. In the reference [12], it is possible that multiple charging effects were taking place in experiments, but not accounted for in the data processing, leading to the apparent monotonically increasing particle yield curve. Our observed particle photoelectric yield

$y_{particle}$ profiles in Figure 3a and b show peaks around 5.64 eV, for both spheres and aggregates. It has been suggested that the turning point on the particle photoelectric yield profile can be related to the surface plasmon resonance [7,27]. However, this seems an unlikely explanation since the peak in our measurements is well above the bulk silver SPR of 3.75 eV. An exact theory for this behavior is not clear and remains an open issue.

3.2. Particle work function

The above Fowler equation (Eq. (2)) has been widely used in particle photoelectric emission studies. Schmidt-ott et al. observed an enormous enhancement on the photoelectric constant c for small particles, and the obtained particle work function was slightly higher than the bulk and vary depending on particle sizes [3]. Wood [28] pointed out that this shift from bulk work function for small metallic spheres has a classical interpretation based on classical image and Coulomb potentials of spherical geometry:

$$\Phi = \Phi_\infty + \frac{e^2}{4\pi\varepsilon_0}\left(\frac{q+1}{r} - \frac{5}{8r}\right) \tag{4}$$

This model agrees with Schmidt-ott's measurement very well. Here in Eq. (4) Φ_∞ is the work function of a flat surface, r is particle radius and q is the initial charges carried by the particle. In the case of single charged particles ($q = 0$), particle size is the only variable, and by expressing particle work function in the unit of eV, Eq. (4) becomes:

$$\Phi = \Phi_\infty + \frac{1.08}{D(nm)}(eV) \tag{5}$$

where D is the diameter of the spheres in the unit of nm. This classical image and Coulomb potentials model can explain the size dependence of particle work function for spheres. However, the work function of aggregates has not been explored so far. Here, we would like to present our investigation on the work function of aggregates.

Combining Eq. (2) and Eq. (3), the particle work function can be extracted from mobility measurement using:

$$\left(\frac{CE}{I}\right)^{\frac{1}{2}} \propto (h\nu - \Phi) \tag{6}$$

An additional point to note is that, strictly speaking, Eq. (2) and thus Eq. (6) are only valid at temperature $T = 0$ K, it is in fact a simplified form of the complete Fowler law. At finite temperature, the complete Fowler law is:

$$\log\left(\frac{Y}{T^2}\right) = B + \log f\left(\frac{h\nu - \Phi}{k_B T}\right) \tag{7}$$

where B is a constant and function f is a known function [2]. The plot of $\log(Y/T^2)$ vs. $(h\nu - \Phi/k_B T)$ is known as the 'Fowler plot' and a fit of data to Eq. (7) yields the work function. The work function extracted through the 'Fowler plot', by definition, is the thermionic work function. As noted by Fowler, the extracted value of work function using the complete Fowler law should be independent of the temperature if the theory were exact [2]. In other words, the 'Fowler plot' approach is to use the measurement at finite temperature to extract work function at $T = 0$ K. As such, works that purport to have investigated temperature effects on photoionization threshold through this approach, would seem to be inappropriate [29,30].

The Fowler–Nordheim Eq. (2) has been widely used and shows excellent agreement with experimental data in various works [3,7,31]. Therefore, we chose to use the Eq. (6) to extract the particle work function. Based on this method, we obtained the particle work function for spheres and aggregates in the mobility size range

15–90 nm, as shown in y-axis of Figure 4. It is obvious from the Figure 4 that the work function of aggregates and spheres are distinctively different. The work function of spheres is clearly size dependent, showing a significant decreasing trend from 4.31 to 4.26 eV as mobility size increases from 15 to 80 nm. To determine the flat surface work function, we use Eq. (5) to fit the data for spheres and obtain the solid line in Figure 4, which gives a flat surface work function of 4.25 eV, and in good agreement with the literature reported bulk value of 4.26 eV [1].

On the other hand, the work function of aggregates, although arguably also decreasing with increasing aggregate mobility size, is certainly less size dependent than spheres. To explain this result, we need to examine particle structure and its relation to particle mobility. The mobility size of sphere is equivalent to its geometric diameter. The fact that our result for spheres shows good agreement with Eq. (5), and the extracted bulk work function agrees with literature, validates our measurement approach. For the case of aggregates, particles have a typical fractal like long-chain structure as observed from TEM (Figure 2a). In our 'ideal aggregate' model, the aggregates consist of primary particles and for a given growth condition, the resulted primary particle size is essentially constant. In this case, the aggregate mobility is related to the number of primaries per aggregates through a power-law relationship [32]. As we only observed very weak size variation in the work function of aggregates, we speculated that the ionization behavior here is not directly related to the aggregates mobility size. We have tried to fit our aggregate work function data using Eq. (5), which yielded both an inadequate fitted curve and a less accurate bulk surface work function (4.30 eV), indicating a poor correlation of particle work function to the mobility size for aggregates. In fact, if we use the literature reported silver bulk work function (Φ_∞) of 4.26 eV [1] and the primary particle diameter (15 nm), Eq. (5) predicts an work function of 4.33 eV, which is within the measured work function of aggregates (4.34–4.32 eV). The above results imply that the work function of aggregates is determined by its primary particle size, not its aggregate size. The small but experimentally significant drop in work function with increasing mobility size is likely because our aggregates are not 'ideal'. Rather we do observe in the TEM images (Figure 2a) some necking between primaries.

It is well known that the work function of particles of finite size follows the scaling law [26]:

$$\Phi = \Phi_\infty + a \cdot N^{-1/3} \tag{8}$$

where N is number of atoms, and a is a constant. Base on this scaling law, a plot of particle work function vs. $1/D_V$ (D_V is the volume
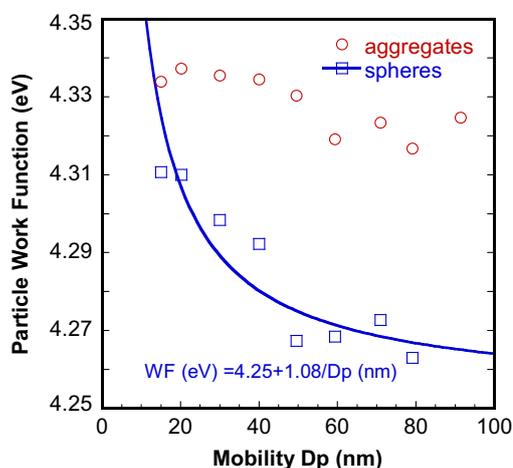

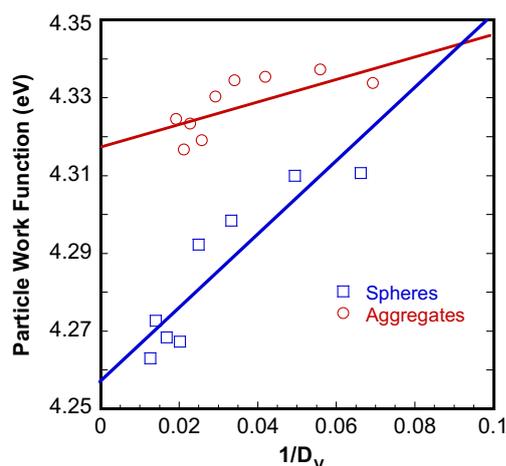**Figure 4.** Particle work function measured for spheres and aggregates.

Figure 5. Particle work function vs. $1/D_V$ for spheres and aggregates, D_V is the volume equivalent diameter.

equivalent diameter, which is proportional to $N^{1/3}$) should give a linear relationship and shown in Figure 5. For spherical particles, the volume equivalent diameter D_V, is equivalent to the particle mobility diameter. The volume equivalent diameter of aggregates can be obtained by estimating the number of primaries particles from the particle mobility [32].

Figure 5 shows that the work function of spheres is linear with inverse D_V and as expected, the deduced bulk work function is close to 4.26 eV, consistent with the result shown in Figure 4 and literature reported values [1]. This is not a surprise since Eq. (8) is equivalent to Eq. (5) for spheres. By contrast, the aggregate data show much less variation as well as a less accurate bulk work function value of ~4.32 eV, which is similar to what we have seen in the analysis of Figure 4. It is interesting to note that the constant a in Eq. (8) is material dependent, in this regard the scaling law would predict the same particle work function regardless of particle structure as long as the number of constituting atoms are the same. Clearly the experimentally measured work function contradicts this. Furthermore, the linear fitted lines for spheres and aggregates intersect at ~4.34 eV, which is very close to the work function of a 15 nm spherical particle (4.33 eV). Thus, Eq. (8) for aggregates should be evaluated based on the number of atoms in the primary particle rather than the whole aggregate. We can conclude that the aggregate structure as a whole plays little or no role in the work function, which is controlled by the primary particle size. However, the reader should not imply from this result that UV charging behavior of aggregates is solely controlled by the primary particle size. Particle UV charging kinetics will be presented in a subsequent work and it is shown that the interactions between primaries do have effect on aggregate photoelectric charging behavior.

4. Conclusions

This letter reports size resolved particle work function measurement of silver nanoparticles in the aerosol phase. The aggregate work function was evaluated for the first time. Our result confirmed that the Fowler–Nordheim law, with the classical image and coulomb potentials model, is applicable to not only spheres but also aggregates. However in the case of aggregates it is the primary particle size that is the relevant size metric in controlling particle work function. We also evaluated the particle photoelectric yield as function of incident photon energy, and showed that discrepancies in results observed in the literature may be attributed to multiple charging effects.

References

[1] H.B. Michaelson, Journal of Applied Physics 48 (1977) 4729.
[2] R.H. Fowler, Physical Review 38 (1931) 45.
[3] A. Schmidt-ott, P. Schurtenberger, H.C. Siegmann, Physical Review Letters 45 (1980) 1284.
[4] A. Keller, M. Fierz, K. Siegmann, H.C. Siegmann, A. Filippov, Journal of Vacuum Science & Technology A: Vacuum Surfaces and Films 19 (2001) 1.
[5] F. Zasada, P. Stelmachowski, G. Maniak, J.F. Paul, A. Kotarba, Z. Sojka, Catalysis Letters 127 (2009) 126.
[6] A.P. Weber, M. Seipenbusch, G. Kasper, Journal of Physical Chemistry A 105 (2001) 8958.
[7] K. Wong, C. Kasperovich, G. Tikhonov, V.V. Kresin, Applied Physics B: Lasers and Optics 73 (2001) 407.
[8] T. Reiners, H. Haberland, Physical Review Letters 77 (1996) 2440.
[9] E. Hontanon, F.E. Kruis, Aerosol Science and Technology 42 (2008) 310.
[10] A. Maisels, F. Jordan, H. Fissan, Journal of Applied Physics 91 (2002) 3377.
[11] D. Matter, M. Mohr, W. Fendel, A. Schmidtott, H. Burtscher, Journal of Aerosol Science 26 (1995) 1101.
[12] U. Muller, H. Burtscher, A. Schmidt-ott, Physical Review B 38 (1988) 7814.
[13] H. Burtscher, L. Scherrer, H.C. Siegmann, A. Schmidt-Ott, B. Federer, Journal of Applied Physics 53 (1982) 3787.
[14] J.K. Jiang, C.J. Hogan, D.R. Chen, P. Biswas, Journal of Applied Physics (2007) 102.
[15] X.F. Ma, M.R. Zachariah, Journal of Physical Chemistry C 113 (2009) 14644.
[16] L. Zhou, A. Rai, N. Piekiel, X. Ma, M.R.J. Zachariah, Journal of Physical Chemistry C 112 (2008) 16209.
[17] K. Ehara, C. Hagwood, K.J. Coakley, Journal of Aerosol Science 27 (1996) 217.
[18] K.J. Higgins, H.J. Jung, D.B. Kittelson, J.T. Roberts, M.R. Zachariah, Journal of Physical Chemistry A 106 (2002) 96.
[19] E.O. Knutson, K.T. Whitby, Journal of Aerosol Science 6 (1975) 443.
[20] M. Shrivastava, A. Gidwani, H.S. Jung, Aerosol Science and Technology 43 (2009) 1218.
[21] C.N. Berglund, W.E. Spicer, Physical Review 136 (1964) A1030.
[22] C.N. Berglund, W.E. Spicer, Physical Review 136 (1964) A1044.
[23] Q.Y. Chen, C.W. Bates, Physical Review Letters 57 (1986) 2737.
[24] W. Kin, V.K. Vitaly, The Journal of Chemical Physics 118 (2003) 7141.
[25] U. Muller, A. Schmidt-ott, H. Burtscher, Zeitschrift Fur Physik B: Condensed Matter 73 (1988) 103.
[26] M. Seidl, K.H. Meiwesbroer, M. Brack, Journal of Chemical Physics 95 (1991) 1295.
[27] R.J. Whitefie, J.J. Brady, Physical Review Letters 26 (1971) 380.
[28] D.M. Wood, Physical Review Letters 46 (1981) 749.
[29] K. Reuter-Hack, G. Kasper, A.P. Weber, Applied Physics A: Materials Science & Processing 95 (2009) 629.
[30] K. Wong, G. Tikhonov, V.V. Kresin, Physical Review B 66 (2002) 125401.
[31] B. Schleicher, H. Burtscher, H.C. Siegmann, Applied Physics Letters 63 (1993) 1191.
[32] W.G. Shin, G.W. Mulholland, S.C. Kim, J. Wang, M.S. Emery, D.Y.H. Pui, Journal of Aerosol Science 40 (2009) 573.